Int. J. Sci. R. Tech., 2026 3(2)
A Multidisciplinary peer-reviewed Journal
www.ijsrtjournal.com [ISSN: 2394-7063]

Original Article

Mechanistic Insights into the OH-Initiated Oxidation of $CF_3C(O)CH_2COCH_3$: A Quantum Study

Narendra Pramanik[1], Devaprasad Deb[1], Nand Kishor Gour[2], Bhupesh Kumar Mishra*[3]

[1]*Department of Chemistry, Himalayan University, Jollang-791109, Arunachal Pradesh, India*
[2]*Department of Chemical Sciences, Tezpur University, Tezpur, Napaam, Assam – 784 028, India*
[3]*Department of Chemistry, Dera Natung Government College, Itanagar- 791113, Arunachal Pradesh, India*

ABSTRACT

A detailed quantum chemical study was carried out to unravel the reaction mechanism, kinetics, and thermochemistry governing the gas-phase oxidation of 1,1,1-trifluoro-pentane-2,4-dione ($CF_3C(O)CH_2C(O)CH_3$, TFP) by hydroxyl (OH) radicals, employing the M06-2X density functional. The most thermodynamically stable conformer of TFP was identified under ambient conditions. Two predominant hydrogen-abstraction channels were characterized, both involving the formation of pre-reactive complexes, thereby indicating an indirect abstraction mechanism. Temperature-dependent rate coefficients for these pathways were computed for the first time over the 250–450 K temperature range using Canonical Transition State Theory (CTST). Based on the calculated kinetic parameters, the atmospheric lifetime of TFP was estimated to be approximately 30.44 days.

Keywords: Fluorinated diketone, DFT, Rate constant, Atmospheric life time

INTRODUCTION

Environmental attention to the atmospheric behavior and transformation of volatile organic compounds (VOCs) emitted from human activities has intensified in recent years, largely as a consequence of rapid population expansion and industrial development. Following their release, VOCs are removed from the troposphere through multiple pathways, including physical processes such as wet and dry deposition, as well as chemical degradation driven by atmospheric oxidation. Photooxidative reactions initiated by hydroxyl (•OH) radicals, chlorine (•Cl) atoms, nitrate (NO_3) radicals, and ozone (O_3) represent the dominant chemical loss mechanisms and typically proceed via hydrogen abstraction or addition to unsaturated carbon bonds. Oxygenated volatile organic compounds (OVOCs), which arise both from primary emissions and secondary oxidation processes, are central to atmospheric photochemistry. Ketones constitute a significant subgroup of oxygenated volatile organic compounds (OVOCs) and originate from both anthropogenic and natural sources, including industrial processes, vehicular emissions [1-3], and the metabolic breakdown of biomass. In the atmosphere, ketones are primarily removed through photolytic processes that generate reactive radical species or via reactions with reactive oxygen species (ROS), leading to the formation of aldehydes, organic acids, and other low-volatility products. Fluorinated diketones (FDKs) are widely utilized in the synthesis of pharmaceuticals, advanced dyes, surface coatings, and metallurgical applications, where they frequently serve as chelating agents [4]. Certain industrial uses, particularly those involving metal–organic chemical vapor deposition techniques, represent potential emission sources of these compounds into the atmosphere [5]. The presence of both carbon–fluorine bonds and carbonyl functional groups in FDKs suggests that they may exhibit non-negligible global warming potential. Among these compounds, kinetic investigations of the reaction between 1,1,1-trifluoro-pentane-2,4-dione (TFP) and hydroxyl (OH) radicals have been experimentally reported. Lego *et al.* [6] determined a value of $(1.3\pm 0.5)\times10^{-11}$ cm^3 $molecule^{-1}$ s^{-1} at (298 ± 2) K by FTIR spectroscopy and $(1.3 \pm 0.2) \times 10^{-11}$ cm^3 $molecule^{-1}$ s^{-1} by using GC-FID chromatography technique. However, despite these

Relevant conflicts of interest/financial disclosures: The authors declare that the research was conducted in the absence of any commercial or financial relationships that could be construed as a potential conflict of interest.

experimental efforts, a detailed theoretical description of the oxidation mechanism of TFP initiated by OH radicals is still lacking. In this context, the present study aims to provide a comprehensive mechanistic and kinetic characterization of the OH-initiated oxidation of TFP using advanced quantum chemical methodologies. Based on the above discussion, the objective of this study is to explore the oxidation mechanism and kinetic parameters of TFP using a robust quantum chemical methodology. The oxidation process is initiated by OH radicals through hydrogen atom abstraction, which can occur at the $–CH_3$ or $–CH_2$ positions of TFP, giving rise to two alternative reaction channels as given in Scheme 1

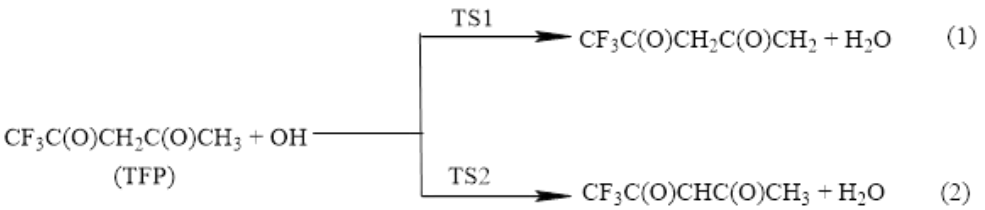

Scheme 1: Oxidation of TFP initiated by OH radical

In the present study, density functional theory (DFT) calculations were carried out to evaluate the energetic profiles, optimized geometries, and harmonic vibrational frequencies of the reactants, products, and transition states associated with the hydrogen-abstraction reactions of TFP.

1. Computational Methods

All electronic structure computations were carried out using the Gaussian 09 software package [7]. Density functional theory (DFT) calculations were performed employing the M06-2X hybrid functional [8] in conjunction with the 6-31+G(d,p) basis set. The M06-2X functional is well recognized for its reliable performance in predicting thermochemical properties and reaction kinetics and has demonstrated good agreement with experimental and theoretical results in numerous prior studies [9-14]. Harmonic vibrational frequency analyses were conducted at the same level of theory to characterize the nature of the optimized stationary points and to obtain zero-point energy corrections. These calculations confirmed that stable species correspond to true minima with no imaginary frequencies, whereas each transition state exhibits a single imaginary frequency associated with the reaction coordinate. Intrinsic reaction coordinate (IRC) calculations [15] were further performed to ensure that each transition state properly connects the relevant reactant and product minima. Using the optimized geometries obtained at the M06-2X/6-31+G(d,p) level, more accurate single-point energy calculations were subsequently carried out with the larger 6-311++G(3df,3pd) basis set, and the resulting energies were used to evaluate the relative energy differences (ΔE) among all stationary points.

RESULTS AND DISCUSSION

At the M06-2X/6-31+G(d,p) level, the calculated thermodynamic data for the species has been recorded in Table 1. The reaction enthalpies (Δ_rH°) and free energies (Δ_rG°) at 298 K for loss processes (1–2) are documented in Table 1. These thermodynamic functions were determined with thermal corrections to the energy at 298 K. The calculated $\Delta_rH°$ and $\Delta_rG°$ values at 298 K indicate that the decomposition pathways taken into consideration in this investigation are feasible and spontaneous. It is evident from Table 1 that the reaction channel 2 is more thermodynamically viable. Because $\Delta_rH^\circ_{298} < 0$, the results also show that reaction channels (1–2) are exothermic in nature. In order to identify, the most stable conformer of TFP scan calculation has been performed by rotating dihedral angle (C6-C5-C1-C12) and the most stable conformer of TFP has taken in consideration for further study. The result obtained during scan calculation has been depicted in Fig. 1. For the hydrogen abstraction reactions, we have considered two reaction routes (1–2), mainly hydrogen abstraction from the $–CH_3$ group and $–CH_2$ group. Pre-reactive complexes (RC1 and RC2) have been found in the entrance channel for reactions (1–2) in the current investigation. The exit channel also contains product complexes, referred to as PC1 and PC2, before the final product is distributed. When TFP and the OH radical interact weakly through hydrogen bonds between C-H...O and OH...O, these

RC complexes are formed. In pre-reactive complexes, hydrogen bonds are formed between the oxygen atom in the hydroxyl radical and the hydrogen atom in TFP. The presence of post-reaction complexes (PC1 and PC2) with energies lower than the corresponding products is also indicated by the comparatively strong C–H–O and O –H–O bonds in reaction channels (1–2). Therefore, it is clear that the reaction route (1-2) may employ indirect procedures. The least energy path was used to find stationary point on a relaxed potential energy surface. Figure 1 shows the electronic structure of the optimized geometry of the reactant, products, hydrogen-bonded reaction complexes, product complexes, and transition states that were produced at the M06-2X/6-31+G(d,p) level. For the reaction channels (1–2), transition states TS1, and TS2 were optimized on the relaxed potential energy surface. The C–H bond of the departing hydrogen and the newly generated bond between the H and O atoms in the OH radical are crucial structural characteristics that must be monitored throughout the development of transition states. The breaking C–H bond length (C12–H13) is 11.06% greater than the observed C–H bond length in the isolated TFP molecule, while the forming O...H bond length is 32.88% longer than the O–H bond length in H_2O, according to a visualization of the optimized structures of TS1 for reaction 1. In the optimized geometry of TS2, the length of the C–H (C5–H3) bond has increased from 1.098 to 1.184 Å while the forming O...H bond length is 42.11% longer than the O–H bond length in H_2O. The barrier of the reactions (1-2) is close to the matching reactants because the elongation of the forming bond is greater than that of the breaking bond. This suggests that an early transition state structure will be used for the reaction, in accordance with Hammond's postulate [16] which applies to exothermic hydrogen abstraction processes. Table 2 presents the results of the harmonic vibrational frequency calculation at the M06-2X/6-31+G(d,p) level. Each transition state has one imaginary frequency due to its first order saddle point character, while the analysis of the harmonic vibrational frequency of minima including reactants, reactant complexes (RCs), product complexes (PCs), and products (P1 and P2) revealed no imaginary frequency (NIMAG = 0). The O16–H13 and C12–H13 stretching modes are represented by the imaginary frequency of TS1 for reaction channel (1), which is 1460 cm^{-1}. This also shows a considerable curvature in the potential energy surface (PES) surrounding the transition state. The imaginary frequency for the hydrogen abstraction from the $–CH_2$ group involving TS2 is determined to be –1096 cm^{-1}, which corresponds to the stretching modes for hydrogen transfer reactions O16–H3 and C5–H3. The representation of the normal-mode corresponding to the calculated imaginary frequencies shows a clear transition state geometry connecting reactants and products during transition. To further ascertain whether a transition state exists on the potential energy surface, the intrinsic reaction coordinate (IRC) calculation [15] is performed at the same theoretical level using the Gonzalez-Schlegel steepest descent path in the mass-weighted Cartesian coordinates with a step size of 0.01($amu^{1/2}$- bohr). Additional proof that the transition state truly connects the intended reactant and product along the corresponding potential energy surface is given by the results of IRC calculations, which are shown in Figure 3. Table 3 summarizes the energy of each optimized geometry used in this study, which was determined using the M06-2X/6-311++G(3df,3pd) method. We employed the species optimal geometries, M06-2X/6-31+G(d,p), for the energetic computation. Using frequency calculation data at the M06-2X/6-31+G(d,p) level of theory, optimization was carried out to compute zero-point energy for stationary points. Zero-point energy (ZPE) were corrected with a scale factor of 0.967 [17] and the total energies of each species were calculated on potential energy surface. Figure 4 shows a schematic potential energy profile of TFP reactivity with the OH radical that was acquired at the M06-2X level using zero-point energy (ZPE) corrections. Zero-point energy corrected total energy has been used for the construction of the energy diagram. The ground state energy of TFP + OH, which includes ZPE, is plotted against these energies, with zero being used randomly. For TS1 and TS2, the energy barrier determined at the M06-2X/6-311++G(3df,3pd) level is 1.82 and 0.73 kcal mol^{-1}, respectively. For the two channels of H-abstraction by OH from TFP, the transition states resides above the reactants by 1.82 and 0.73 kcal mol^{-1}, for reaction routes (1-2), respectively.

3.1 Kinetics calculation

The conventional transition state theory (CTST) [18] and Eckart's tunneling correction [19] were used to calculate the rate coefficient values for various reaction channels spanning the 250–450 K temperature range using the following formula.

$$k = \sigma\Gamma(T)\frac{k_B T}{h}\frac{Q^{\ddagger}_{TS}}{Q_R}\exp\frac{-\Delta E}{RT} \qquad (3)$$

The σ represents symmetry factor whereas tunneling correction factor at temperature T is represented by the symbol Γ(T). The total partition functions (per unit volume) for the reactants and transition states are denoted by Q_R and $Q^{\ddagger}_{TS}$,, respectively. R stands for the universal gas constant, k_B for the Boltzmann constant, h for Planck's constant, and ΔE for the barrier height incorporating zero-point energy correction. The value of symmetry factor for reaction channels (1–2) has been taken as 3 and 2, respectively. The tunneling correction factor for two reaction channels at 298 K is found to be 11.01 and 3.54, respectively. The obtained rate coefficients in the temperature range of 250 – 450 K for reaction pathways (1–2) are recorded in Table 4. At 298 K, our calculated rate constants for TS1 and TS2 were found to be $7.59\times10^{-14}$and 1.14×10^{-13}cm^3 molecule^{-1} s^{-1} respectively at M06-2X/6-31++G(3df,3pd) level of theory. The computed overall k_{OH} value at 298K is found to be 1.90×10^{-13} cm^3 molecule^{-1} s^{-1}for TFP with OH reaction. Our calculated rate constant for the reaction of TFP with OH radical is in good agreement with the reported value of 0.18×10^{-12} cm^3 molecule^{-1} s^{-1} according to the Structure-Activity Relationships (SAR), calculated by the AOPWIN v.4.11 software [20] for the keto form of TFP. However, our calculated value of rate constant for the titled reaction is in line with the experimental value of (1.3± 0.4) $\times10^{-11}$ cm^3 molecule^{-1} s^{-1} at (298 ± 2) K by Lugo et al. [6] The percentage branching ratios for each of the reaction channels determined at 298 K are found to be 39.93 and 60.07 %, respectively. From these results, it can be emphasize that the hydrogen abstraction from the –CH_2 group is kinetically more advantageous than the other reaction pathway i.e. abstraction from –CH_3 group.

3.2 Atmospheric lifetime

The atmospheric lifetime of TFP (τ_{eff}) can be estimated by assuming that its removal from the atmosphere occurs primarily through the reaction with OH radicals. Then τ_{eff} can be expressed as: [21]

$$\tau_{eff} \approx \tau_{OH}$$

where τ_{OH} = ($k_{OH}\times$ [OH])$^{-1}$ and [OH]$^{-1}$ represents global average concentration in atmosphere. Taking the global mean atmospheric OH radical concentration of 2.0×10^6 molecules cm^{-3} and k_{OH} value at 298 K as 1.9×10^{-13} cm^3 molecule^{-1} s^{-1}, the atmospheric lifetime of TFP is estimated to be 30.44 days.

CONCLUSIONS

In summary, the present study provides a comprehensive potential energy surface and rate constant data for the atmospheric and environmental consequence of TFP molecule initiated by OH radical by employing M06-2X/6-31+G(d,p) level of theory. We have done various inquires involving the optimization of structural parameters, energy profiles, thermochemistry, and kinetics of the TFP with OH radical. For that, we have identified two reaction channels which follow an indirect path through the formation of pre- and post- reaction complexes on the potential energy surface. All rate constants, computed by canonical transition state theory are in reasonable agreement with the limited experimental data. The thermal rate constant for the H atom abstraction of TFP by OH radicals is found to be 1.90×10^{-13} cm^3 molecule^{-1} s^{-1} at 298 K. The calculated branching ratios for two reaction channels are found to be 39.93 % and 60.07 % respectively at 298 K. Our results suggest that hydrogen abstraction from the –CH_2 group is likely the dominant route for OH-initiated oxidation of TFP under reaction conditions. The atmospheric lifetime for TFP molecule is estimated to be 30.44 days.

Conflicts of interest

The authors declare no conflicts of interest.

ACKNOWLEDGMENTS

The authors acknowledge financial support from the Department of Science and Technology, New Delhi in the form of project under DST-SERB CRG scheme.

REFERENCE

1. Bouzidi, H., Djehiche, M., Coddeville, P., Fittschen, C., Tomas, A., Atmospheric Chemistry of α-Diketones: Kinetics of C5 and C6 Compounds with Cl Atoms and OH Radicals, Int J Chem Kin, 2017, 49(2):112-118. https://doi.org/10.1002/kin.21060
2. Yujing, M., Mellouki, A. The near-UV absorption cross sections for several ketones, J. Photochem, Photobiol. A: Chem. 2000, 134:31-36. https://doi.org/10.1016/S1010-6030(00)00243-4
3. Gierczak, T., Buckholder, J.B., Bauerle, S., Ravishankara, A.R. Photochemistry of acetone under tropospheric conditions. Chem Phys Lett 1998, 231:229-244. https://doi.org/10.1016/S0301-0104(98)00006-8
4. Ilmi, R., Haque, A. AI-Busaidi, I.J., AI Rasbi, N.K., Khan, M. S. Synthesis and photophysical properties of hetero trinuclear complexes of tris B-diketonate Europium with organoplatinum chromophore. Dyes Pigments, 2019, 162, 59-66.
5. Bareño, V.D. O., Santos, D. S., Frigo, L. M., de Mello, D. L., Malavolta, J. L., Blanco, R. F., Pizzuti, L., Flores, D.C., Flores, A. F. C. An Acetal Acylation Methodology for Producing Diversity of Trihalomethyl 1,3-dielectrophiles and 1,2-Azole Derivatives, J. Braz. Chem. Soc. 2020, 31(2): 244-264. https://doi.org/10.21577/0103-5053.20190160
6. Lugo, P. L., Straccia, V.G., Rivela, C. B., Klotz, I. P., Illmann, N., Teruel, M. A., Wiesen, P., Blanco, M. B. Diurnal photodegradation of fluorinated diketones (FDKs) by OH radicals using different atmospheric simulation chambers: Role of keto-enol tautomerization on reactivity, Chemosphere 2022, 286 (1):131562.
7. Frisch, M. J.; et al. Gaussian 09, Revision B.01; Gaussian, Inc.: Wallingford, CT.;2010.
8. Zhao, Y.; Truhlar, D. G. The M06 Suite of Density Functionals for Main Group Thermochemistry, Thermochemical Kinetics, Noncovalent Interactions, Excited States and Transition Elements: Two New Functionals and Systematic Testing of Four M06-Class Functionals and 12 Other Functionals. Theor. Chem. Acc. 2006, 120:215-241.
9. Gour, N. K.; Borthakur, K.; Paul, S.; Deka, R. C. Tropospheric degradation of 2-fluoropropene (CH3CFCH2) initiated by hydroxyl radical: Reaction mechanisms, kinetics and atmospheric implications from DFT study, Chemosphere, 2020, 238, 124556.
10. Lily, M.; Baidya, B.; Chandra, A. K. Dual level direct dynamics study of gas phase reaction of CF3CH2OCH2CF3 with Cl atoms and atmospheric degradation of CF3CH2OCH2CF3, Chem. Phys. Lett. 2017, 669:211–217.
11. Rao, P. K.; Deka, R. C.; Gour N. K.; Gejji, S. P. Understanding the Atmospheric Oxidation of HFE-7500 (C3F7CF(OC2H5) CF(CF3)2) Initiated by Cl Atom and NO3 Radical from Theory, J. Phys. Chem. A, 2018, 122:6799–6808.
12. Baidya, B.; Lily, M.; Patgiri, D.; Hynniewta, S.; Chandra, A. K. CHF2CF2OCHF2: conformational analysis and direct dynamics study of its reaction with Cl atoms and atmospheric fate, New J. Chem. 2020, 44, 4276-4284.
13. Paul, S.; Mishra, B. K.;Baruah, S. D.; Deka, R. C.; Gour. N. K. Atmospheric oxidation of HFE-7300 [n-C2F5CF(OCH3) CF(CF3)2] initiated by •OH/Cl oxidants and subsequent degradation of its product radical: a DFT approach. Env. Sci. Poll. Res. 2020, 27 (1): 907-920.
14. Gour, N. K.; Mishra, B. K.;Sarma, P. J.; Begum, P.; Deka, R. C. Tropospheric degradation of HFE-7500[n-C3F7CF(OCH2CH3)CF(CF3)2]initiated by OH radicals and Fate of alkoxy radical [n-C3F7CF(OCH(O)CH3)CF(CF3)2]: A DFT investigation, J. Fluor. Chem. 2017, 204:11–17.
15. Gonzalez, C.; Schlegel, H. B. An improved algorithm for reaction path following: higher–order implicit algorithms, J. Chem. Phys. 1989, 90, 2154−2161.
16. G.S. Hammond, A Correlation of Reaction Rates, J. Am. Chem. Soc. 1955, 77:334-338. https://doi.org/10.1021/ja01607a027
17. I. M. Alecu, J. Zheng, Y. Zhao, D. G. Truhlar, Computational Thermochemistry: Scale Factor Databases and Scale Factors for Vibrational Frequencies Obtained from Electronic Model Chemistries, J. Chem. Theory Comput. 2010, 6:2872-2887.

18. Laidler, K. J. Chemical Kinetics, 3rd edn. Pearson Education, New Delhi (2004).
19. Xiao, R.; Noerpel, M.; Luk, H.L.; Wei, Z.; Spinney, R. Thermodynamic and kinetic study of ibuprofen with hydroxyl radical: A density functional theory approach, Int. J. Quant. Chem. 2014,114:74-83.
20. Kwok, E.S.C., Atkinson, R. Estimation of hydroxyl radical reaction rate constants for gas-phase organic compounds using a structure-reactivity relationship: An update, Atmos. Environ. 1995, 29 (14):1685-1695. https://doi.org/10.1016/1352-2310(95)00069-B
21. Kurylo, M. J., Orkin, V.L. Determination of Atmospheric Lifetimes via the Measurement of OH Radical Kinetics, Chem. Rev. 2003, 103(12): 5049–5076. https://doi.org/10.1021/cr020524c.

HOW TO CITE: Narendra Pramanik, Devaprasad Deb, Nand Kishor Gour, Bhupesh Kumar Mishra*, Mechanistic Insights into the OH-Initiated Oxidation of $CF_3C(O)CH_2COCH_3$: A Quantum Study, Int. J. Sci. R. Tech., 2026, 3 (2), 9-17. https://doi.org/10.5281/zenodo.18466050

Table1. Thermochemical data for reaction channels (1-2) calculated at M06-2X/6-31+G(d,p) level of theory. All values are in kcal mol-1

Reaction channels	$\Delta_rH°$	$\Delta_rG°$
Reaction 1	–21.28	–21.02
Reaction 2	–22.40	–22.51

Table 2 Harmonic vibrational frequencies of reactants, transition states and products at M06-2X/6-31+G(d,p) level of theory.

Species	Vibrational Frequencies (cm^{-1})
$CF_3C(O)CH_2C(O)CH_3$	18, 31, 50, 104, 148, 215, 225, 324, 372, 424, 489, 499, 532, 581, 624, 722, 815, 828, 885, 1025, 1036, 1068, 1182, 1227, 1256, 1278, 1326, 1396, 1409, 1438, 1476, 1482, 1872, 1910, 3074, 3079, 3132, 3153, 3197
TS1	1460i, 20, 37, 44, 65, 119, 167, 189, 228, 292, 328, 359, 412, 426, 489, 504, 521, 581, 622, 701, 769, 816, 844, 893, 907, 1027, 1056, 1083, 1184, 1229, 1232, 1274, 1276, 1326, 1406, 1435, 1445, 1495, 1843, 1909, 3072, 3121, 3137, 3198, 3729
TS2	1096i, 35, 44, 54, 83, 92, 124, 151, 215, 223, 237, 326, 381, 430, 496, 505, 528, 585, 615, 675, 728, 822, 827, 922, 932, 1036, 1053, 1073, 1215, 1223, 1249, 1276, 1315, 1340, 1405, 1412, 1475, 1478, 1861, 1899, 3075, 3142, 3155, 3201, 3761
RC1	27, 36, 46, 66, 90, 135, 167, 176, 225, 229, 330, 384, 427, 458, 494, 502, 531, 544, 584, 627, 728, 817, 829, 900, 1026, 1046, 1064, 1176, 1232, 1264, 1278, 1328, 1399, 1411, 1438, 1475, 1498, 1847, 1911, 3075, 3077, 3133, 3160, 3177, 3663
RC2	48, 56, 66, 81, 93, 139, 144, 171, 218, 233, 274, 327, 369, 382, 429, 493, 507, 533, 585, 618, 724, 822, 825, 892, 1027, 1038, 1070, 1179, 1238, 1259, 1283, 1312, 1400, 1411, 1433, 1472, 1486, 1869, 1890, 3074, 3078, 3129, 3155, 3194, 3745
PC1	27, 28, 47, 63, 119, 144, 168, 224, 232, 252, 333, 381, 395, 405, 430, 494, 526, 538, 547, 591, 626, 733, 813, 847, 889, 931, 1045, 1057, 1177, 1231, 1281, 1313, 1345, 1408, 1437, 1504, 1607, 1652, 1909, 3066, 3142, 3195, 3320, 3772, 3986
PC2	26, 38, 42, 52, 126, 134, 166, 194, 236, 249, 262, 282, 309, 331, 368, 442, 511, 518, 527, 595, 665, 736, 796, 840, 884, 1027, 1033, 1113, 1227, 1273, 1292, 1331, 1408, 1460, 1462, 1474, 1603, 1737, 1759, 3084, 3160, 3199, 3249, 3855, 3987
H_2O	1596, 3885, 4010
$CF_3C(O)CH_2COCH_2$	26, 48, 73, 138, 209, 230, 329, 371, 417, 428, 495, 516, 540, 588, 624, 729, 780, 838, 881, 930, 1033, 1054, 1166, 1230, 1282, 1307, 1329, 1406, 1441, 1485, 1661, 1906, 3073, 3148, 3207, 3328
$CF_3C(O)CHCOCH_3$	38, 43, 87, 122, 129, 219, 246, 311, 350, 435, 507, 513, 544, 587, 647, 734, 785, 854, 896, 998, 1036, 1109, 1208, 1217, 1285, 1350, 1404, 1457, 1479, 1482, 1746, 1794, 3074, 3148, 3198, 3225

Table 3 Relative energies (in kcal mol^{-1}) with zero-point energy correction for the reactants, reaction complexes, transition states, product complexes and products at M06-2X/6-311++G(3df,3pd) level of theory.

Species	M06-2X/6-311++G(3df,3pd)
TFP+ OH	0.00
RC1	–3.27
RC2	–4.81
TS1	1.82
TS2	0.73
PC1	–27.75
PC2	–32.19
P1 + H_2O	–21.90
P2 + H_2O	–23.70

Table 4: Rate constants of different reaction channels and overall rate constant (in cm^3 molecule^{-1} s^{-1}) within the temperature range of 250–450 K at M06-2X/6-311++G(3df,3pd) level of theory.

Rate constant	250 K	298.15 K	300 K	350 K	400 K	450 K
k_1	8.44×10^{-14}	7.59×10^{-14}	7.57×10^{-14}	7.99×10^{-14}	8.96×10^{-14}	1.03×10^{-13}
k_2	1.35×10^{-13}	1.14×10^{-13}	1.13×10^{-13}	1.12×10^{-13}	1.14×10^{-13}	1.27×10^{-13}
$k_{overall}$	4.38×10^{-13}	1.90×10^{-13}	1.89×10^{-13}	1.92×10^{-13}	2.04×10^{-13}	2.30×10^{-13}

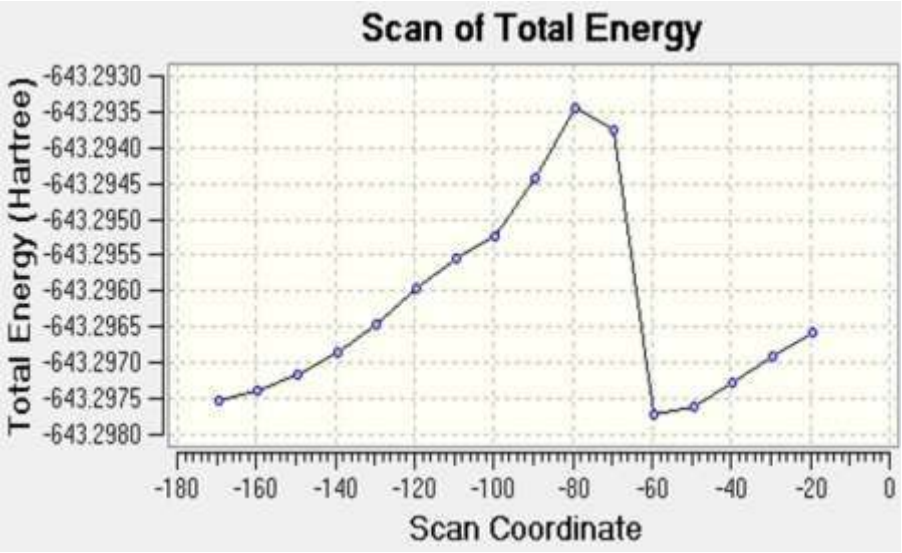

Fig. 1: The electronic energy of different conformers of TFP vs. dihedral angle C- C□C□C at M06-2X/6-31+G(d,p) level of theory

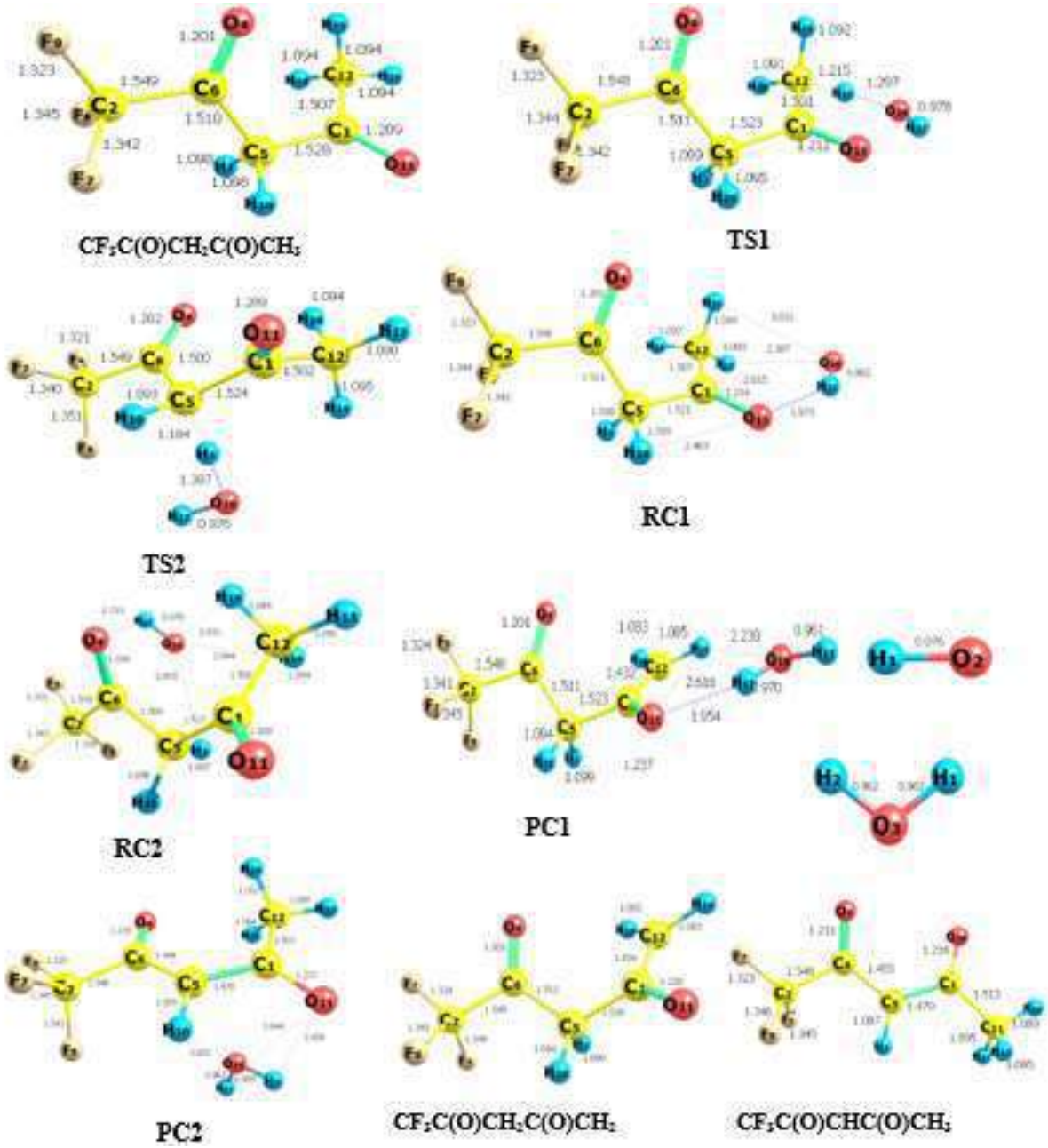

Fig. 2: Optimized geometry of reactants, reaction complexes, transition states, product complexes and products obtained at M06-2X/6-31+G(d,p) level of theory. Bond lengths are in angstroms.

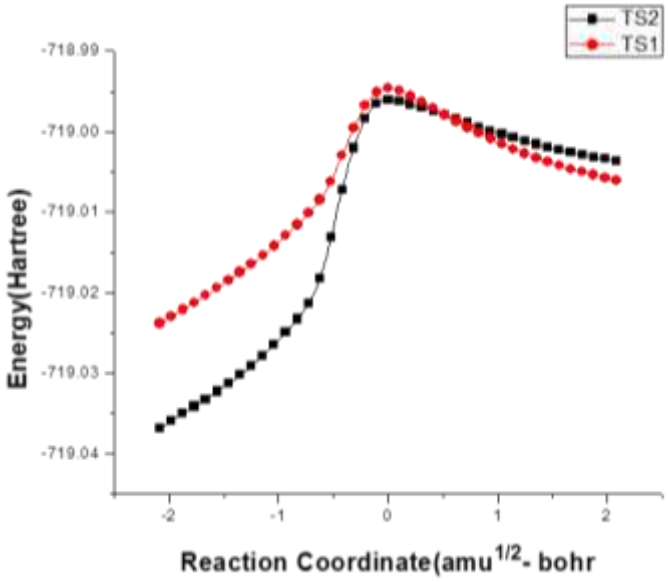

Fig.3: IRC plots performed for transition states TS1 and TS2obtained at M06-2X/6-31+G(d,p) level of theory.

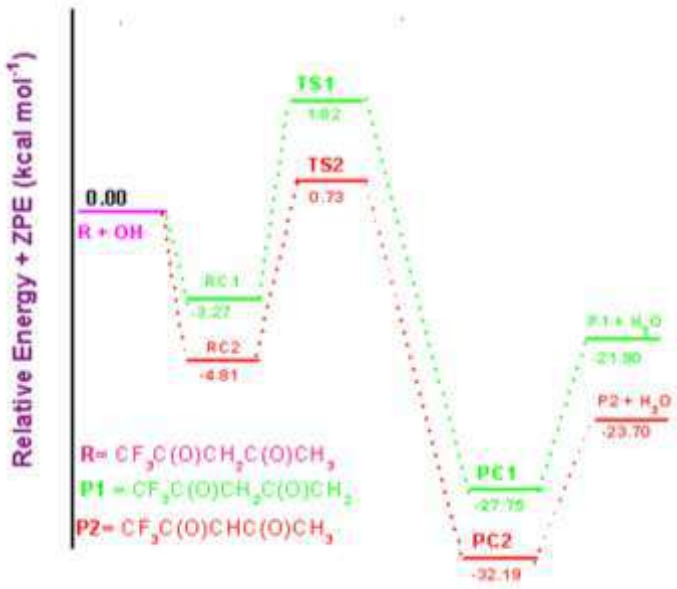

Fig. 4: Potential energy diagram for the reaction of OH radical with TFP at M06-2X/6-311++G(3df,3pd) level of theory